

## Dynamic Atomic Reconstruction: How Fe<sub>3</sub>O<sub>4</sub> Thin Films Evade Polar Catastrophe for Epitaxy

C. F. Chang,<sup>1</sup> Z. Hu,<sup>1</sup> S. Klein,<sup>2,\*</sup> X. H. Liu,<sup>1</sup> R. Sutarto,<sup>2,†</sup> A. Tanaka,<sup>3</sup> J. C. Cezar,<sup>4,‡</sup> N. B. Brookes,<sup>4</sup> H.-J. Lin,<sup>5</sup> H. H. Hsieh,<sup>6</sup> C. T. Chen,<sup>5</sup> A. D. Rata,<sup>1,§</sup> and L. H. Tjeng<sup>1</sup>

<sup>1</sup>Max Planck Institute for Chemical Physics of Solids, Nöthnitzer Straße 40, 01187 Dresden, Germany

<sup>2</sup>II. Physikalisches Institut, Universität zu Köln, Zùlpicher Str. 77, 50937 Köln, Germany

<sup>3</sup>Department of Quantum Matter, ADSM, Hiroshima University, Higashi-Hiroshima 739-8530, Japan

<sup>4</sup>European Synchrotron Radiation Facility, 71 Avenue des Martyrs, 38000 Grenoble, France

<sup>5</sup>National Synchrotron Radiation Research Center, 101 Hsin-Ann Road, Hsinchu 30077, Taiwan

<sup>6</sup>Chung Cheng Institute of Technology, National Defense University, Taoyuan 335, Taiwan

(Received 14 September 2015; published 18 October 2016)

Polar catastrophe at the interface of oxide materials with strongly correlated electrons has triggered a flurry of new research activities. The expectations are that the design of such advanced interfaces will become a powerful route to engineer devices with novel functionalities. Here, we investigate the initial stages of growth and the electronic structure of the spintronic Fe<sub>3</sub>O<sub>4</sub>/MgO (001) interface. Using soft x-ray absorption spectroscopy, we have discovered that the so-called A-sites are completely missing in the first Fe<sub>3</sub>O<sub>4</sub> monolayer. This discovery allows us to develop an unexpected but elegant growth principle in which, during deposition, the Fe atoms are constantly on the move to solve the divergent electrostatic potential problem, thereby ensuring epitaxy and stoichiometry at the same time. This growth principle provides a new perspective for the design of interfaces.

DOI: 10.1103/PhysRevX.6.041011

Subject Areas: Condensed Matter Physics,  
Materials Science, Spintronics

Physical properties of surfaces and interfaces of solids could markedly differ from those in the bulk, especially in cases when the surface or interface involves non-neutral crystal planes. For insulators, these polar planes cause the electrostatic potential to diverge and thus to destabilize the system dramatically. The surface or interface is then forced to reconstruct, for example, by forming facets or defects. Or more spectacularly, it could give up a substantial amount of charge, thereby altering its electronic structure completely [1–3]. Recently, claims have been made that this happens at the SrTiO<sub>3</sub>/LaAlO<sub>3</sub> interface since the interface is conducting while the two constituents are good insulators separately [4,5]. In fact, the formation of a two-dimensional electron gas and the occurrence of superconductivity in

this interface have generated frantic efforts worldwide to explore the potential of these interfaces for device applications [6–12], as well as to search for new emergent phenomena such as quantum criticality in two-dimensional electron gas systems [13–15]. However, the growth process of these interfaces and polar interfaces, in general, is a mystery. How do the atoms rearrange themselves during the deposition or growth such that a well-ordered and smooth interface is formed, despite the destabilizing forces due to the catastrophic electrostatic potential? Understanding the growth principles will widen the scope of interfaces that one may want to design: Interfaces that appear impossible to grow at first sight may now be tried.

Here, we investigate the polar interface between Fe<sub>3</sub>O<sub>4</sub> and the MgO (001) substrate, one of the most used interfaces in the research field of spintronics [16–24]. This interface is completely not understood in terms of atomic structure, electronic structure, and growth mode. Figures 1(a) and 1(b) illustrate how the Fe<sub>3</sub>O<sub>4</sub> inverse spinel crystal structure, consisting of Fe<sup>3+</sup> ions in tetrahedral coordination (A-sites), and Fe<sup>2+</sup> and Fe<sup>3+</sup> ions (or, on average, Fe<sup>2.5+</sup>) in octahedral coordination (B-sites) with O<sup>2-</sup> ions in a fcc lattice, builds up the polar catastrophe problem. We have prepared the system using molecular beam epitaxy (MBE). This deposition method allows for a layer-by-layer growth of the Fe<sub>3</sub>O<sub>4</sub> under ultrahigh vacuum conditions, which facilitates the use of *in situ* characterization techniques with surface monolayer (ML) sensitivity.

\*Present address: Institute of Materials Physics in Space, German Aerospace Center, Linder Hohe, 51147 Köln, Germany.

†Present address: Canadian Light Source, Saskatoon, Saskatchewan S7N 2V3, Canada.

‡Present address: National Center for Research in Energy and Materials, Brazilian Synchrotron Light Laboratory, C.P. 6192, 13083-970, Campinas, SP, Brazil.

§Present address: Institute of Physics, Martin Luther University, Halle-Wittenberg, 06099 Halle, Germany.

Published by the American Physical Society under the terms of the Creative Commons Attribution 3.0 License. Further distribution of this work must maintain attribution to the author(s) and the published article's title, journal citation, and DOI.

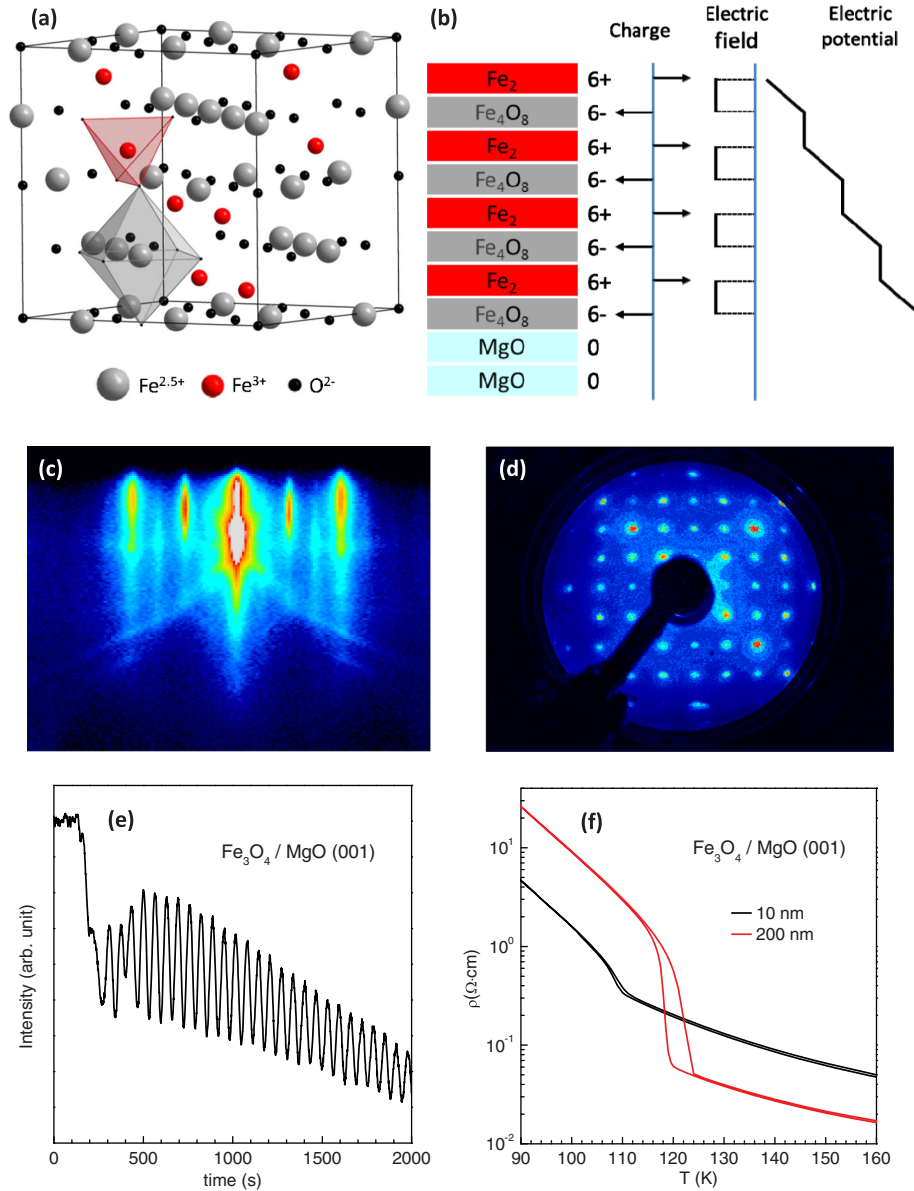


FIG. 1.  $\text{Fe}_3\text{O}_4$  on  $\text{MgO}$  (001). (a) Structure of  $\text{Fe}_3\text{O}_4$ . (b) Buildup of the polar catastrophe of  $\text{Fe}_3\text{O}_4$  on  $\text{MgO}$  (001): charged planes, and the corresponding charge, electric field, and electric potential. (c,d) RHEED and LEED patterns, respectively, of a 200-nm epitaxial  $\text{Fe}_3\text{O}_4$  (001) film showing the characteristic  $(\sqrt{2} \times \sqrt{2})\text{R}45^\circ$  superstructure. (e) RHEED intensity oscillations of the specularly reflected beam. The electron beam was incident along the  $[100]$  direction, with a primary energy of 20 kV. (f) Resistivity as a function of temperature of a 10-nm and a 200-nm thin film, showing the presence of the Verwey transition.

The MBE growth of  $\text{Fe}_3\text{O}_4$  on  $\text{MgO}$  (001) is also known to produce films with excellent physical properties [22]. In order to obtain direct insight into the atomic and electronic structure of the interface, we utilize soft x-ray absorption spectroscopy (XAS) at the Fe  $L_{2,3}$  edges. This spectroscopic technique is extremely sensitive to the local coordination and charge state of the Fe ions [25–28].

$\text{Fe}_3\text{O}_4$  thin films with thicknesses varying between 0.67 and 8 ML were grown on  $\text{MgO}$  (001). Each film was grown on a new and freshly annealed substrate. The substrate temperature was kept at 250 °C during the growth in order to avoid the Mg interdiffusion at the  $\text{Fe}_3\text{O}_4/\text{MgO}$

interface [29,30]. Details about the film growth are given in Ref. [31]. One ML consists of one (001)-oriented layer of oxygen anions together with the appropriate number of Fe cations to maintain charge neutrality and stoichiometry, and it has a thickness of 2.1 Å. In Figs. 1(c) and 1(d), we present representative reflection high-energy electron diffraction (RHEED) and low-energy electron diffraction (LEED) patterns, respectively, of a 200-nm-thick  $\text{Fe}_3\text{O}_4$  film to demonstrate that the surface is still smooth for very long deposition times. The typical  $(\sqrt{2} \times \sqrt{2})\text{R}45^\circ$  surface reconstruction is also clearly visible. Figure 1(e) shows the regular oscillations with time in the intensity of

the specularly reflected RHEED beam during growth, indicating a two-dimensional layer-by-layer growth mode. Figure 1(f) displays the resistivity as a function of temperature from a 10-nm and a 200-nm film, showing the presence of the characteristic Verwey transition [22].

Figure 2 depicts the room-temperature Fe  $L_3$  XAS spectra of  $\text{Fe}_3\text{O}_4$  films with thicknesses varying from 0.67 ML to 8 ML, and of a  $\text{Fe}_3\text{O}_4$  bulk single crystal. A  $\text{Fe}_2\text{O}_3$  single crystal was measured simultaneously in a separate chamber to serve as energy reference for a Fe  $L_3$  edge. Further XAS experimental details and display of the entire Fe  $L_{2,3}$  spectral range are given in Fig. S1 of Ref. [31]. We also include in Fig. 2 the spectra of bulk  $\text{YBaCo}_3\text{FeO}_7$  [28], bulk FeO (reproduced from Ref. [32]) and bulk  $\text{Fe}_2\text{O}_3$  as references for  $\text{Fe}^{3+}$  ions in tetrahedral coordination,  $\text{Fe}^{2+}$  ions in octahedral coordination, and  $\text{Fe}^{3+}$  ions in octahedral coordination, respectively. The line shapes of the spectra strongly depend on the multiplet

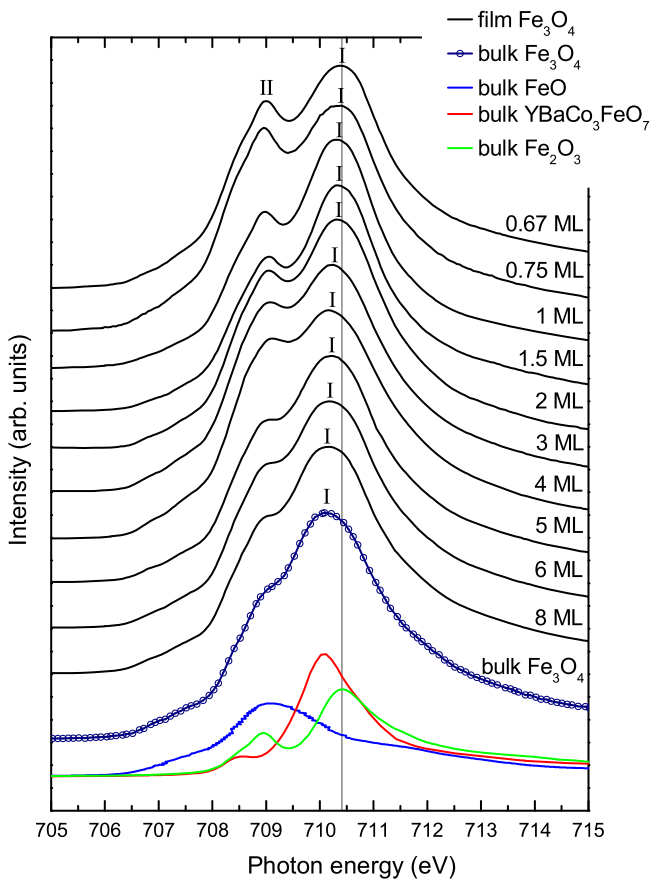


FIG. 2. Fe  $L_3$  XAS spectra of  $\text{Fe}_3\text{O}_4$  films. The film thickness varies from 0.67 to 8 ML. The reference spectra of bulk  $\text{Fe}_3\text{O}_4$ , bulk  $\text{YBaCo}_3\text{FeO}_7$  ( $\text{Fe}^{3+}$  in tetrahedral coordination) [28], bulk FeO ( $\text{Fe}^{2+}$  in octahedral coordination) [32], and bulk  $\text{Fe}_2\text{O}_3$  ( $\text{Fe}^{3+}$  in octahedral coordination) are also included. All spectra were measured at 300 K. The gray line indicates the energy position of the main peak in the spectrum of bulk  $\text{Fe}_2\text{O}_3$ . The full Fe  $L_{2,3}$  spectral range is presented in Ref. [31].

structure given by the atomiclike Fe  $3d - 3d$  and  $2p - 3d$  Coulomb and exchange interactions, as well as by local crystal fields and the hybridization with the O  $2p$  ligands [25–28]. Here, we note the striking similarities of the spectral features of the 8-ML  $\text{Fe}_3\text{O}_4$  thin film and the bulk magnetite, which confirms that our  $\text{Fe}_3\text{O}_4$  films have the correct stoichiometry.

We now focus on the thickness dependence of the spectra. Clear and systematic changes can be observed, in particular, in the peak position of the spectral feature labeled as (I) and in the intensity of the spectral feature labeled as (II) relative to that of peak (I) (see Fig. 2). The position of peak (I) of the thinnest  $\text{Fe}_3\text{O}_4$  films, i.e., of the 0.67, 0.75, and 1-ML films, is the same as that of bulk  $\text{Fe}_2\text{O}_3$ , while for the thicker films, i.e., 2 ML and beyond, it is more similar to that of bulk  $\text{YBaCo}_3\text{FeO}_7$ . This gives a first indication that the thinnest films contain only tiny amounts of  $\text{Fe}^{3+}$  ions in tetrahedral coordination and implies that such A-site Fe ions could essentially only be present for films of 2-ML thickness and beyond. This would then also explain why for the thinnest films one can see two separate peaks (I) and (II) like in bulk  $\text{Fe}_2\text{O}_3$  (green curve), while for thicker films, the appearance of an in-between peak associated with the  $\text{Fe}^{3+}$  ions in tetrahedral coordination (red curve) will fill up the valley between peak (I) and (II), causing peak (II) to become a shoulder and the position of the larger peak (I) to shift to lower energies. It is important to note that the foot at the onset of the Fe  $L_3$  edge, i.e., the feature between 706 and 707.7 eV, which is part of the spectral feature characteristic for  $\text{Fe}^{2+}$  ions in octahedral B sites (see blue curve), is thickness independent. All these ideas strongly suggest that the spectral weight of the A-site and the B-site  $\text{Fe}^{3+}$  ions varies strongly with thickness.

To interpret and better understand the XAS spectra and their thickness dependence, we have performed calculations using the well-established configuration interaction cluster model, which includes the full atomic multiplet theory and the local effects of the solid [25–28]. We have simulated each of the XAS spectra shown in Fig. 2 and obtained the spectral weight of the different Fe sites; computational details and fits are given in Refs. [31] and [33], and in Figs. S2–S4 of Ref. [31]. The results are plotted as closed squares in the top panel of Fig. 3, where the error bars reflect the deviations of the fits to the experimental data. From the relative concentrations of the constituents, we have calculated the average valence, or, equivalently, by taking the oxygen lattice to be complete, we have determined the Fe content  $y$  in our  $\text{Fe}_y\text{O}$  films. These  $y$  values are plotted as black closed squares in the bottom panel of Fig. 3. We can observe that all points are very close to the  $\text{Fe}_{3/4}\text{O}$  (gray) line, which confirms the correct stoichiometry of our films through the entire thickness range and is very consistent with the RHEED intensity oscillations that have a constant time period, i.e., independent of the film thickness.

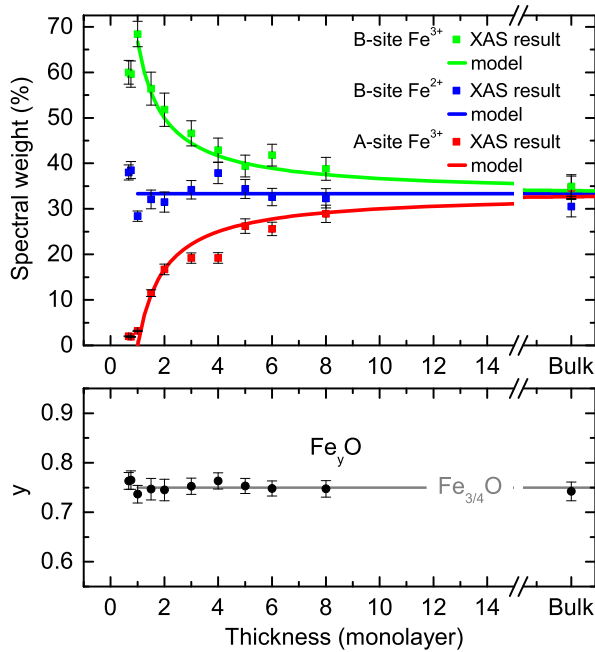


FIG. 3. The extracted spectral weight of each Fe site versus the film thickness. The spectral weight of the B-site Fe<sup>3+</sup>, the B-site Fe<sup>2+</sup>, and the A-site Fe<sup>3+</sup> are given by the green, blue, and red squares, respectively. Green, blue, and red curves depict the concentrations of the B-site Fe<sup>3+</sup>, the B-site Fe<sup>2+</sup>, and the A-site Fe<sup>3+</sup>, respectively, in our model (see the text). The Fe content ( $y$ ) of the Fe <sub>$y$</sub> O films derived from the average valence is shown in the bottom panel. The error bars reflect the deviations of the fits to the experimental data.

An important aspect that emerges directly from the simulations is the strong thickness dependence of the different Fe constituents (see Fig. 3). We recall that bulk Fe<sub>3</sub>O<sub>4</sub> has 1/3 (33%) Fe<sup>3+</sup> ions in tetrahedral coordination (A-sites), and 1/3 (33%) Fe<sup>2+</sup> and 1/3 (33%) Fe<sup>3+</sup> ions in octahedral coordination (B-sites). To our surprise, we found that the amount of A-site Fe<sup>3+</sup> ions is practically negligible for the thinnest films, i.e., 2%–3% instead of the 33% bulk value. At the same time, the amount of B-site Fe<sup>3+</sup> in the thinnest films is between 60% and 68%, much larger than the 33% bulk value. We also observe that with increasing film thickness, the A-site Fe<sup>3+</sup> amount increases and the B-site Fe<sup>3+</sup> decreases, both approaching the 33% bulk value; see, for example, the 8-ML results in Fig. 3. Interestingly, the amount of B-site Fe<sup>2+</sup> is rather constant, and independent of the film thickness, it fluctuates around the 33% bulk value.

These spectroscopic findings provide crucial data for the determination of the actual growth process and the interface structure. In particular, the observation that the first monolayer of the Fe<sub>3</sub>O<sub>4</sub> film has essentially no A-sites is a surprising piece of information. In fact, as far as the monolayer is concerned, the choice of “nature” not to have A-sites is the simplest way to solve the planar electrostatic

potential problem. As can be seen from Figs. 1(a) and 1(b), it is indeed the presence of the A-sites that causes the polar catastrophe to occur, as there are no negative ions in those A-site planes to neutralize the charges. Thus, since there are no A sites for the first monolayer, there is no electrostatic problem. Then, the first monolayer basically constitutes a charge-neutral nonpolar rocksalt FeO layer with 25% Fe vacancies. All Fe ions occupy the B-site, with 33% of them having a 2+ valence and 67% a 3+ state; the vacancies are not ordered since we did not observe any superstructure. We have also carried out polarization-dependent XAS measurements, and we are indeed able to verify in detail that the dichroic spectrum is also consistent with the 33% Fe<sup>2+</sup> and 67% Fe<sup>3+</sup> B-site occupation. See Fig. S5 of Ref. [31]. Please note that these XAS spectra and the dichroism therein are very different from those of Fe atoms on MgO [34]. Moreover, capping this monolayer with a thick layer of MgO induces spectral weight changes that are fully consistent with the presence of 25% Fe vacancies. See Refs. [31] and [33], and Fig. S6 of Ref. [31].

For the second monolayer, in the experiment, we observe the appearance of some amount of A-sites, about 16.7%; see top panel of Fig. 3. We now arrive at the following model, Fig. 4, where the left side shows the growth process and the right side the corresponding net charges, electric field, and electric potential of each plane. Since in bulk magnetite a monolayer per unit cell includes two A-site Fe<sup>3+</sup>, two B-site Fe<sup>2+</sup>, two B-site Fe<sup>3+</sup>, and eighth oxygen ions, we use the formula notation Fe<sub>6</sub>O<sub>8</sub> instead of Fe<sub>3/4</sub>O to describe each monolayer. When deposited, the second monolayer will first form a nonpolar monolayer, like the first monolayer. Then, both the first and the second layers give away one Fe<sup>3+</sup> ion, as shown in Fig. 4(b), to the space in between them to form a layer with two A-site Fe<sup>3+</sup> ions. Then, the entire film also remains nonpolar: A 6+ charged layer is sandwiched by two 3- charged layers. The electric field oscillates symmetrically around zero, and the electric potential remains nullified. In this model, there are two A-sites per 2-ML formula unit; i.e., the A-site concentration is  $2/(2 \times 6) = 16\%$ , which is very close to the experiment. The remaining outer Fe<sub>5</sub>O<sub>8</sub> (defective rocksalt) layers each contain three Fe<sup>3+</sup> and two Fe<sup>2+</sup> B-site ions. The concentration of the Fe<sup>2+</sup> B-site ions is thus  $(2 \times 2)/(2 \times 6) = 33\%$ , i.e., the same as for the first monolayer and consistent with the experiment; see top panel of Fig. 3.

For a 3-ML film, the layer added will again form a nonpolar monolayer first. This monolayer and the subsurface monolayer then carry out the same process in which both give away one Fe<sup>3+</sup> ion to the space in between. See Fig. 4(c). Again, the potential divergence remains nullified after this process, as shown on the rightmost panel of Fig. 4(c). One complete bulk Fe<sub>6</sub>O<sub>8</sub> layer is now formed. This growth process is repeated for the subsequent layers, and the model predicts that the concentration of the A-site ions will increase following the geometrical series

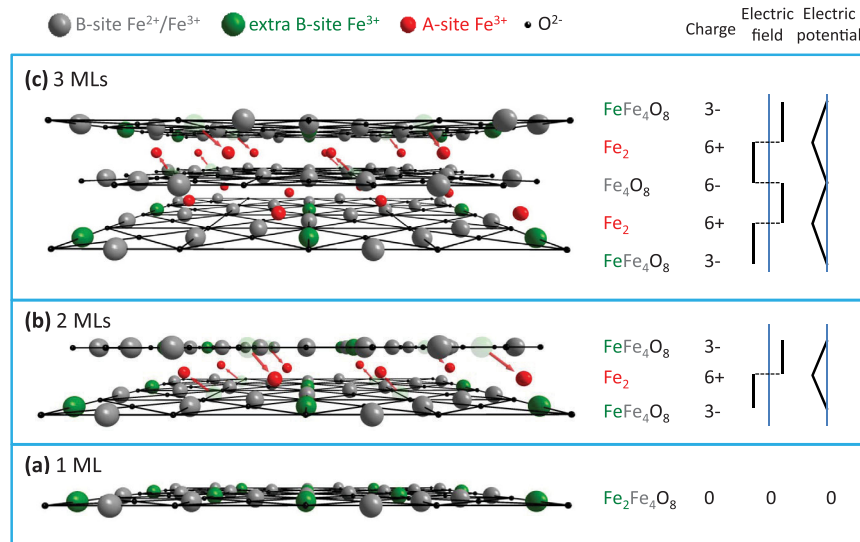


FIG. 4. Model for the growth process of polar  $\text{Fe}_3\text{O}_4$  (001) thin films. (a) One monolayer, (b) two monolayers, and (c) three monolayers.

$2(n-1)/6n$ , while the concentration of the  $\text{Fe}^{2+}$  B-site ions will remain constant at  $2n/6n = 33\%$  and that of the  $\text{Fe}^{3+}$  B-site ions will decrease following  $2(n+1)/6n$ , where  $n$  denotes the number of monolayers. These predictions of the model are also presented in Fig. 3. We see that the essential behavior observed in the experiment is well reproduced with convergence to the bulk values for thicker films. We also note that an ordering in the outer  $\text{Fe}_5\text{O}_8$  layer can be made consistent with the often-observed  $(\sqrt{2} \times \sqrt{2})R45^\circ$  surface reconstruction in thicker (001)  $\text{Fe}_3\text{O}_4$  films; see Ref. [31] for details.

We have thus found that the A-sites are absent in the first monolayer or interface, and that Fe ions are on the move while the film is growing to accommodate for the presence of A-sites inside the film having the proper crystal structure and stoichiometry. We clearly have a “dynamic atomic reconstruction” taking place here.

It is interesting to note that the  $\text{Fe}_3\text{O}_4$  thin films are insulating and that the interface does not induce metallicity, as shown by the resistivity measurements displayed in Fig. 1(f). This result is obviously in contrast with the resistivity measurements on  $\text{SrTiO}_3/\text{LaAlO}_3$  [5,35–37] and  $\text{SrTiO}_3/\text{RETiO}_3$  [13–15]. In principle, the  $\text{Fe}_5\text{O}_8$  interface layer could be conducting since this layer can be considered as a defective and doped rocksalt FeO layer. Yet, considering the fact that small polaron effects in bulk  $\text{Fe}_3\text{O}_4$  are strong and that they hamper the conductivity [38–40], we may expect that this will also be the case for the interface layer. Its resistivity will then be dominated by strong scattering effects due to disorder.

Our findings have direct and important implications for the field of  $\text{Fe}_3\text{O}_4$  spintronics. There are some reports concerning the possible existence of a magnetically dead layer at the interface [41–43], but others ascribe the

decrease of the magnetization in the thin films to the presence of antiphase boundaries leading to superparamagnetic behavior of the domains [44–46]. Our findings may give credit to the proponents of the dead magnetic layer model. In view of the absence or a low amount of A-sites in the interface region, some of the superexchange paths that determine the ferrimagnetism in  $\text{Fe}_3\text{O}_4$  are certainly missing. This would also explain why tunneling experiments have spin polarizations that are different than expected from the properties of bulk  $\text{Fe}_3\text{O}_4$  [47]. We can now propose that the insertion of a monolayer of magnetic metals like Fe, Co, Ni, or even noble metals like Cu, Ag, Au, or Pt between the  $\text{Fe}_3\text{O}_4$  and the insulating oxide substrate will drastically change the situation: The metal layer inserted will act as a charge reservoir that can accommodate the flow of planar charges required to stabilize a  $\text{Fe}_3\text{O}_4$  interface layer that has A-sites like in the bulk. The occurrence of a magnetically dead layer can then be prevented, and the spin polarization at the interface can also be increased. A hint that the latter is not unrealistic can be found in an early work by Dedkov *et al.* [48] on oxidized Fe films deposited on metal substrates.

To summarize, using soft x-ray absorption spectroscopy, we find that nature provides us with an unexpected but elegant solution for the polar catastrophe problem at the  $\text{Fe}_3\text{O}_4/\text{MgO}$  (001) interface: The A-site  $\text{Fe}^{3+}$  ions are missing in the first  $\text{Fe}_3\text{O}_4$  layer, and the growth process involves movements of not only the surface but also the subsurface Fe ions, securing epitaxy and stoichiometry at the same time. Having identified this “dynamic atomic reconstruction” growth principle, we conclude that we really have to think differently and openly about how polar interfaces can grow. Apparently, nature offers us a much wider range of opportunities to prepare unstable polar

interfaces. It would be interesting to put effort into growing a monolayer or a few monolayers of  $\text{Fe}_3\text{O}_4$  film where the defects are ordered so that diffraction techniques can confirm the growth model.

The research in Köln was supported by the Deutsche Forschungsgemeinschaft through SFB 608. The research of X. H. L. was supported by the Max Planck-POSTECH Center for Complex Phase Materials.

- 
- [1] A. Zangwill, *Physics at Surfaces* (Cambridge University Press, Cambridge, England, 1988).
- [2] C. Noguera, *Physics and Chemistry at Oxide Surfaces* (Cambridge University Press, Cambridge, England, 1996).
- [3] R. Hesper, L. H. Tjeng, A. Heres, and G. A. Sawatzky, *Photoemission Evidence of Electronic Stabilization of Polar Surfaces in  $\text{K}_3\text{C}_{60}$* , *Phys. Rev. B* **62**, 16046 (2000).
- [4] S. Okamoto and A. J. Millis, *Electronic Reconstruction at an Interface Between a Mott Insulator, and a Band Insulator*, *Nature (London)* **428**, 630 (2004).
- [5] A. Ohtomo and H. Y. Hwang, *A High-Mobility Electron Gas at the  $\text{LaAlO}_3/\text{SrTiO}_3$  Heterointerface*, *Nature (London)* **427**, 423 (2004).
- [6] M. Huijben, A. Brinkman, G. Koster, G. Rijnders, H. Hilgenkamp, and D. H. A. Blank, *Structure-Property Relation of  $\text{SrTiO}_3/\text{LaAlO}_3$  Interfaces*, *Adv. Mater.* **21**, 1665 (2009).
- [7] J. Mannhart and D. G. Schlom, *Oxide Interfaces—An Opportunity for Electronics*, *Science* **327**, 1607 (2010).
- [8] S. A. Chambers, M. H. Engelhard, V. Shutthanandan, Z. Zhu, T. C. Droubay, L. Qiao, P. V. Sushko, T. Feng, H. D. Lee, T. Gustafsson, E. Garfunkel, A. B. Shah, J.-M. Zuo, and Q. M. Ramasse, *Instability, Intermixing and Electronic Structure at the Epitaxial  $\text{LaAlO}_3/\text{SrTiO}_3$  (001) Heterojunction*, *Surf. Sci. Rep.* **65**, 317 (2010).
- [9] S. A. Chambers, *Understanding the Mechanism of Conductivity at the  $\text{LaAlO}_3/\text{SrTiO}_3$  (001) Interface*, *Surf. Sci.* **605**, 1133 (2011).
- [10] H. Y. Hwang, Y. Iwasa, M. Kawasaki, B. Keimer, N. Nagaosa, and Y. Tokura, *Emergent Phenomena at Oxide Interfaces*, *Nat. Mater.* **11**, 103 (2012).
- [11] M. Salluzzo, S. Gariglio, X. Torrelles, Z. Ristic, R. Di Capua, J. Drnec, M. Moretti Sala, G. Ghiringhelli, R. Felici, and N. B. Brookes, *Structural and Electronic Reconstructions at the  $\text{LaAlO}_3/\text{SrTiO}_3$  Interface*, *Adv. Mater.* **25**, 2333 (2013).
- [12] A. Janotti, L. Bjaalie, L. Gordon, and C. G. Van de Walle, *Controlling the Density of the Two-Dimensional Electron Gas at the  $\text{SrTiO}_3/\text{LaAlO}_3$  Interface*, *Phys. Rev. B* **86**, 241108 (2012).
- [13] P. Moetakef, D. G. Ouellette, J. R. Williams, S. James Allen, L. Balents, D. Goldhaber-Gordon, and S. Stemmer, *Quantum Oscillations from a Two-Dimensional Electron Gas at a Mott/Band Insulator Interface*, *Appl. Phys. Lett.* **101**, 151604 (2012).
- [14] C. A. Jackson, J. Y. Zhang, C. R. Freeze, and S. Stemmer, *Quantum Critical Behaviour in Confined  $\text{SrTiO}_3$  Quantum Wells Embedded in Antiferromagnetic  $\text{SmTiO}_3$* , *Nat. Commun.* **5**, 4258 (2014).
- [15] S. Raghavan, J. Y. Zhang, and S. Stemmer, *Two-Dimensional Electron Liquid at the (111)  $\text{SmTiO}_3/\text{SrTiO}_3$  Interface*, *Appl. Phys. Lett.* **106**, 132104 (2015).
- [16] R. A. de Groot, F. M. Mueller, P. G. van Engen, and K. H. J. Buschow, *New Class of Materials: Half-Metallic Ferromagnets*, *Phys. Rev. Lett.* **50**, 2024 (1983).
- [17] A. Yanase and K. Siratori, *Band Structure in the High Temperature Phase of  $\text{Fe}_3\text{O}_4$* , *J. Phys. Soc. Jpn.* **53**, 312 (1984).
- [18] S. A. Chambers, *Epitaxial Growth and Properties of Thin Film Oxides*, *Surf. Sci. Rep.* **39**, 105 (2000).
- [19] M. Ziese, *Extrinsic Magnetotransport Phenomena in Ferromagnetic Oxides*, *Rep. Prog. Phys.* **65**, 143 (2002).
- [20] R. Pentcheva, F. Wendler, H. L. Meyerheim, W. Moritz, N. Jedrecy, and M. Scheffler, *Jahn-Teller Stabilization of a Polar Metal Oxide Surface:  $\text{Fe}_3\text{O}_4$  (001)*, *Phys. Rev. Lett.* **94**, 126101 (2005).
- [21] Jean-B. Moussy, *From Epitaxial Growth of Ferrite Thin Films to Spin-Polarized Tunneling*, *J. Phys. D* **46**, 143001 (2013).
- [22] X. H. Liu, A. D. Rata, C. F. Chang, A. C. Komarek, and L. H. Tjeng, *Verwey Transition in  $\text{Fe}_3\text{O}_4$  Thin Films: Influence of Oxygen Stoichiometry and Substrate-Induced Microstructure*, *Phys. Rev. B* **90**, 125142 (2014).
- [23] R. Bliem, E. McDermott, P. Ferstl, M. Setvin, O. Gamba, J. Pavelec, M. A. Schneider, M. Schmid, U. Diebold, P. Blaha, L. Hammer, and G. S. Parkinson, *Subsurface Cation Vacancy Stabilization of the Magnetite(001) Surface*, *Science* **346**, 1215 (2014).
- [24] Scott A. Chambers, *Stability at the Surface*, *Science* **346**, 1186 (2014).
- [25] F. M. F. de Groot, *J. Electron Spectrosc. Relat. Phenom.* **67**, 529 (1994).
- [26] A. Tanaka and T. Jo, *Resonant 3d, 3p and 3s Photoemission in Transition Metal Oxides Predicted at 2p Threshold*, *J. Phys. Soc. Jpn.* **63**, 2788 (1994).
- [27] T. Burnus, Z. Hu, Hua Wu, J. C. Cezar, S. Niitaka, H. Takagi, C. F. Chang, N. B. Brookes, H.-J. Lin, L. Y. Jang, A. Tanaka, K. S. Liang, C. T. Chen, and L. H. Tjeng, *X-Ray Absorption and X-Ray Magnetic Dichroism Study on  $\text{Ca}_3\text{CoRhO}_6$  and  $\text{Ca}_3\text{FeRhO}_6$* , *Phys. Rev. B* **77**, 205111 (2008).
- [28] N. Hollmann, Z. Hu, M. Valldor, A. Maignan, A. Tanaka, H. H. Hsieh, H.-J. Lin, C. T. Chen, and L. H. Tjeng, *Electronic and Magnetic Properties of the Kagome Systems  $\text{YBaCo}_4\text{O}_7$  and  $\text{YBaCo}_3\text{MO}_7$  ( $M = \text{Al}, \text{Fe}$ )*, *Phys. Rev. B* **80**, 085111 (2009).
- [29] Y. J. Kim, Y. Gao, and S. A. Chambers, *Selective Growth and Characterization of Pure, Epitaxial  $\alpha\text{-Fe}_2\text{O}_3$  (0001) and  $\text{Fe}_3\text{O}_4$  (001) Films by Plasma-Assisted Molecular Beam Epitaxy*, *Surf. Sci.* **371**, 358 (1997).
- [30] J. F. Anderson, M. Kuhn, U. Diebold, K. Shaw, P. Stoyanov, and D. Lind, *Surface Structure and Morphology of Mg-Segregated Epitaxial  $\text{Fe}_3\text{O}_4$  (001) Thin Films on  $\text{MgO}$  (001)*, *Phys. Rev. B* **56**, 9902 (1997).
- [31] See Supplemental Materials at <http://link.aps.org/supplemental/10.1103/PhysRevX.6.041011> for details of the thin film growth, the XAS experimental details

- and the entire Fe L<sub>2,3</sub> spectral range, the XAS spectra computational details, and the  $(\sqrt{2} \times \sqrt{2})R45^\circ$  surface reconstruction, which is consistent with the Fe<sub>5</sub>O<sub>8</sub> surface as proposed by our model.
- [32] J. H. Park, Ph.D. thesis, University of Michigan (1994).
- [33] T. Haupricht, R. Sutarto, M. W. Haverkort, H. Ott, A. Tanaka, H. H. Hsieh, H.-J. Lin, C. T. Chen, Z. Hu, and L. H. Tjeng, *Local Electronic Structure of Fe<sup>2+</sup> Impurities in MgO Thin Films: Temperature-Dependent Soft X-Ray Absorption Spectroscopy Study*, *Phys. Rev. B* **82**, 035120 (2010).
- [34] S. Baumann, F. Donati, S. Stepanow, S. Rusponi, W. Paul, S. Gangopadhyay, I. G. Rau, G. E. Pacchioni, L. Gragnaniello, M. Pivetta, J. Dreiser, C. Piamonteze, C. P. Lutz, R. M. Macfarlane, B. A. Jones, P. Gambardella, A. J. Heinrich, and H. Brune, *Origin of Perpendicular Magnetic Anisotropy and Large Orbital Moment in Fe Atoms on MgO*, *Phys. Rev. Lett.* **115**, 237202 (2015).
- [35] M. Huijben, G. Rijnders, D. H. A. Blank, S. Bals, S. V. Aert, J. Verbeeck, G. V. Tendeloo, A. Brinkman, and H. Hilgenkamp, *Electronically Coupled Complementary Interfaces Between Perovskite Band Insulators*, *Nat. Mater.* **5**, 556 (2006).
- [36] S. Thiel, G. Hammerl, A. Schmehl, C. W. Schneider, and J. Mannhart, *Tunable Quasi-Two-Dimensional Electron Gases in Oxide Heterostructures*, *Science* **313**, 1942 (2006).
- [37] M. P. Warusawithana, C. Richter, J. A. Mundy, P. Roy, J. Ludwig, S. Paetel, T. Heeg, A. A. Pawlicki, L. F. Kourkoutis, M. Zheng, M. Lee, B. Mulcahy, W. Zander, Y. Zhu, J. Schubert, J. N. Eckstein, D. A. Muller, C. Stephen Hellberg, J. Mannhart, and D. G. Schlom, *LaAlO<sub>3</sub> Stoichiometry is Key to Electron Liquid Formation at LaAlO<sub>3</sub>/SrTiO<sub>3</sub> Interfaces*, *Nat. Commun.* **4**, 2351 (2013).
- [38] J.-H. Park, L. H. Tjeng, J. W. Allen, P. Metcald, and C. T. Chen, *Single-Particle Gap above the Verwey Transition in Fe<sub>3</sub>O<sub>4</sub>*, *Phys. Rev. B* **55**, 12813 (1997).
- [39] D. Schrupp, M. Sing, M. Tsunekawa, H. Fujiwara, S. Kasai, A. Sekiyama, S. Suga, T. Muro, V. A. M. Brabers, and R. Claessen, *High-Energy Photoemission on Fe<sub>3</sub>O<sub>4</sub>: Small Polaron Physics and the Verwey Transition*, *Europhys. Lett.* **70**, 789 (2005).
- [40] M. Kimura, H. Fujiwara, A. Sekiyama, J. Yamaguchi, K. Kishimoto, H. Sugiyama, G. Funabashi, S. Imada, S. Iguchi, Y. Tokura, A. Higashiya, M. Yabashi, K. Tamasaku, T. Ishikawa, T. Ito, S. Kimura, and S. Suga, *Polaronic Behavior of Photoelectron Spectra of Fe<sub>3</sub>O<sub>4</sub> Revealed by Both Hard X-Ray and Extremely Low Energy Photons*, *J. Phys. Soc. Jpn.* **79**, 064710 (2010).
- [41] P. A. A. van der Heijden, P. J. H. Bloemen, J. M. Gaines, J. T. W. M. van Eemeren, R. M. Wolf, p. j. van der Zaag, and W. J. M. de Jonge, *Magnetic Interface Anisotropy of MBE-Grown Ultra-Thin (001) Fe<sub>3</sub>O<sub>4</sub> Layers*, *J. Magn. Mater.* **159**, L293 (1996).
- [42] Y. Zhou, C. McEvoy, R. Ramos, and I. V. Shvets, *The Magnetic and Magnetoresistance Properties of Ultrathin Magnetite Films Grown on MgO Substrate*, *J. Appl. Phys.* **99**, 08J111 (2006).
- [43] G. F. M. Gomes, T. E. P. Bueno, D. E. Parreiras, G. J. P. Abreu, A. de Siervo, J. C. Cezar, H.-D. Pfannes, and R. Paniago, *Magnetic Moment of Fe<sub>3</sub>O<sub>4</sub> Films with Thicknesses near the Unit Cell Size*, *Phys. Rev. B* **90**, 134422 (2014).
- [44] M. A. James, F. C. Voogt, L. Niesen, O. C. Rogojuanu, and T. Hibma, *The Role of Interfacial Structure in Determining Magnetic Behaviour in MBE-Grown Fe<sub>3</sub>O<sub>4</sub>/MgO Multilayers on MgO(001)*, *Surf. Sci.* **402-404**, 332 (1998).
- [45] F. C. Voogt, T. T. M. Palstra, L. Niesen, O. C. Rogojuanu, M. A. James, and T. Hibma, *Superparamagnetic Behavior of Structural Domains in Epitaxial Ultrathin Magnetite Films*, *Phys. Rev. B* **57**, R8107 (1998).
- [46] S. K. Arora, H.-C. Wu, R. J. Choudhary, I. V. Shvets, O. N. Mryasov, H. Yao, and W. Y. Ching, *Giant Magnetic Moment in Epitaxial Fe<sub>3</sub>O<sub>4</sub> Thin Films on MgO(100)*, *Phys. Rev. B* **77**, 134443 (2008).
- [47] S. S. P. Parkin and T. Venkatesan (private communication).
- [48] Yu. S. Dedkov, U. Rüdiger, and G. Güntherodt, *Evidence for the Half-Metallic Ferromagnetic State of Fe<sub>3</sub>O<sub>4</sub> by Spin-Resolved Photoelectron Spectroscopy*, *Phys. Rev. B* **65**, 064417 (2002).